

Resolving Microlens Blends Using Image Subtraction

Andrew Gould and Jin H. An

Department of Astronomy, the Ohio State University, 140 W. 18th Ave., Columbus, OH 43210

gould, jinhan@astronomy.ohio-state.edu

ABSTRACT

Blended light is an important source of degeneracy in the characterization of microlensing events, particularly in binary-lens and high magnification events. We show how the techniques of image subtraction can be applied to form an image of the blend with the source removed. In many cases, it should be possible to construct images with very high signal-to-noise ratio. Analysis of these images can help distinguish between competing models that have different blend fractions, and in some cases should allow direct detection of the lens.

Subject headings: astrometry – gravitational lensing – methods: statistical

1. Introduction

Blended light can be a major nuisance in the analysis of microlensing events, leading to degeneracies in the interpretation of the event parameters. On the other hand, if unlensed light were detected and could be attributed with good confidence to the lens itself, this would greatly aid in understanding the physical characteristics of the lens. The analysis of blended light is therefore important in several aspects of microlensing.

In general, microlensing light curves are fit to the functional form,

$$F(t) = F_s A(t) + F_b, \quad A(t) \geq 1, \quad (1)$$

where $F(t)$ is the flux observed as a function of time, F_s is the flux from the lensed source when it is not magnified, F_b is the flux from any light that lies within the point spread function (PSF) but is not magnified during the event, and $A(t)$ is the magnification. The unlensed light F_b could come from the lens itself, from a companion to the lens or to the lensed source whose projected separation is too great for the companion to participate in the event, or from one or more random field stars that happen to be projected close to the line of sight.

When microlensing light curves are fit to models, F_b must be left as an almost completely free parameter. The only constraint is that it cannot be negative. Even this constraint can be violated to a small extent: microlensing events are found in very crowded fields where faint stars are typically separated by less than a PSF and so form part of the “sky”. If statistical fluctuations leave a small hole in this background just at the position of the lensed source, then F_b can be slightly negative.

Blending can be degenerate with parameters of the model that predicts $A(t)$. For example, in point-source/point-lens events there is a continuous degeneracy where higher blending, shorter timescales, and lower source-lens impact parameters all move in tandem. This degeneracy can be resolved with arbitrary precision given arbitrarily good data, but in realistic cases it places significant limits on the precision with which the impact parameter and timescale can be determined. This in turn limits one’s ability to determine the sensitivity of the event to planetary perturbations (Albrow et al. 2001; Gaudi et al. 2001). For binary-lens events, there is often a discrete degeneracy between wide-binary and close-binary solutions, the first example of which (Albrow et al. 1999) was discovered simultaneously with their theoretical prediction (Dominik 1999). These two solutions have substantially different blending parameters F_b , so that if it were possible to rule out (or argue against) one of the two blending parameters, one could also distinguish between the two solutions.

There are several tools currently available to deal with blending. Alard, Mao, & Guibert (1995) showed that if a single unlensed star is offset from the lensed source by θ_b , then it induces an astrometric deviation on the apparent position of the source, which varies with the magnification: $\delta\theta = r\theta_b(1 - A_{\text{ap}}^{-1})$, where $A_{\text{ap}} = (AF_s + F_b)/(F_s + F_b)$ is the apparent

magnification, and $r = F_b / (F_s + F_b)$ is the unlensed fraction of the baseline flux, $F_s + F_b$. This provides a model-independent measure of the parameter combination $r\theta_b$. The ratio of this quantity measured in two bands provides a fourth relation among the four flux quantities (F_s and F_b in each of the two bands), the other three being the two baseline fluxes and the color of lensed source, which can be determined from a simple regression between the fluxes in two bands during the event. Hence, in principle, one can solve for all four quantities. In practice, there can be several stars contributing to the unlensed light, in which case the information extracted by this method would be highly degenerate. If the direction of the astrometric deviation is the same in two bands, this might be taken as an indication that a single star is dominating the unlensed light, but this assumption could be violated if there is another blended source whose position or color is similar to that of the lensed source. Moreover, crowded-field astrometry is intrinsically difficult, so that this method may ultimately be limited in the precision it can reach.

High resolution images by the *Hubble Space Telescope (HST)* have been used to resolve blending by random field stars in 8 microlensing events observed toward the Large Magellanic Cloud (Alcock et al. 2001). This is a very powerful technique because even for relatively crowded fields, the chance is small that a random star will be both bright enough to affect the event and close enough to the lensed source to escape detection. Nevertheless, the method is limited by the restricted availability of *HST* time. In particular, *HST* observations generally cannot be undertaken until after the end of the event when it is too late to influence observational strategy.

Neither of these methods can distinguish between light from the lensed source and unlensed light from the lens itself, nor generally from companions to the lens or the lensed source. However, future high precision astrometric measurements using interferometers such as *Space Interferometry Mission (SIM)* will be able to disentangle these various light sources, even though they will not be able to resolve them (Boden, Shao, & Van Buren 1998; Dominik & Sahu 2000; Jeong, Han, & Park 1999). The principle is essentially the same as that of Alard et al. (1995), but the much higher precision allows one to measure the motion of the centroid of lensed source light, which traces an ellipse. A luminous lens will change the parameters of this elliptical motion in a detectable way (Han & Jeong 1999), and companions to the lens or source will distort the ellipse into other shapes (Han 2001). However, it will probably be at least a decade before this method is used at all, and when it is, it will be feasible only for a relatively few bright events.

Here we present a new method to study blends using image subtraction. There exist many working image subtraction algorithms (Tomaney & Crotts 1996; Alard & Lupton 1998; Alard 2000; Woźniak 2000). All share the same basic approach. One first forms a high-quality “template” from one or several good-seeing images. Then for each other “current” image, one convolves the template to the same seeing as the current image, translates it so the two images are geometrically aligned, and linearly rescales its flux so that they are photometrically aligned as well. In principle, the two images are then identical (up to photon noise) except where sources have varied. Hence when the template is subtracted from the current image, all that remains are a set of (usually) isolated PSF’s at the locations of these variables. Since the difference image has the appearance of a high-Galactic-latitude field, photometry is much easier and more accurate than it is in the original crowded field.

At first sight, it appears that the unlensed light, and with it the blend parameter F_b , disappear from the analysis. In fact, the parameter F_b in equation (1) is replaced by an arbitrary offset in the fit to difference-image photometry, so the degeneracies connected with the blend persist. In fact they are somewhat worsened because, as mentioned above, for crowded-field photometry, one can at least constrain F_b to be non-negative, whereas there are no a priori conditions upon the corresponding difference-imaging offset parameter. However, by doing both types of photometry, and aligning them by linear regression, one can relate the offset parameter to F_b , and so recover this constraint.

The method we propose is to form a linear combination of images such that the lensed source is removed from the resulting image, but all the unlensed sources remain. The images must be geometrically and photometrically aligned and convolved to the same seeing before combining them.

As we describe in § 2, the resulting image of the unlensed sources depends explicitly on $A(t)$, that is, on the model of the microlensing event. Hence, different models that are consistent with the photometric data will lead to different images of the unlensed sources. As we discuss in § 3, some of these images will be implausible, or even physically impossible. When such conflicts exist, they can be used to argue against or rule out certain classes of models, and thus restrict the allowed space of solutions. Some required statistics results are derived in an Appendix.

2. Constructing an Image of the Unlensed Sources

Consider a series of n images $\{I_i(x, y), i = 1, \dots, n\}$, as functions of pixel position (x, y) . For simplicity, we will assume that these images have already been convolved to the same seeing, geometrically aligned, and linearly rescaled, so that they may be directly compared with one another. All the sources in the image will be assumed to be constant, except the microlensed source which varies with magnification $A_i = A(t_i)$. We adopt $A(t)$ from the model of the light curve under consideration. That is, different models lead to different images of the unlensed sources, only one of which can be correct. We show in § 3 how to use the resulting images to distinguish among competing models.

Let $B(x, y)$ be an arbitrary linear combination of images

$$B(x, y) = \sum_{i=1}^n a_i(x, y) I_i(x, y), \quad (2)$$

where the $a_i(x, y)$ are coefficients that vary both as a function of pixel position in the image (x, y) , and as a function of image number i , but subject to the two constraints

$$\sum_{i=1}^n a_i(x, y) = 1; \quad \sum_{i=1}^n a_i(x, y) A_i = 0. \quad (3)$$

Then B will be an image of the field with the lensed source removed. That is, the first constraint insures that all constant sources will be retained in B , while the second insures that the microlensed source will be deleted. With the microlensed source removed from B , the neighboring unlensed sources can be studied more closely.

For the simplest case $n = 2$, the constraints (eqs. [3]) then completely determine the a_i ,

$$a_1(x, y) = \frac{A_2}{A_2 - A_1}; \quad a_2(x, y) = \frac{-A_1}{A_2 - A_1}, \quad (4)$$

which are then independent of position. This implies

$$B = \frac{A_2 I_1 - A_1 I_2}{A_2 - A_1} \quad \text{for } n = 2. \quad (5)$$

Forming B as a combination of only two images may well suffice for many applications. In this case, the images should be chosen to both have very good seeing and very different magnifications. However, there may be other cases where one wants to obtain a higher signal-to-noise ratio (S/N) for B by combining a large number of images. Let $\sigma_i(x, y)$ be the error in $I_i(x, y)$. For example, $\sigma_i(x, y)$ might be given by the photon noise in the (x, y) pixel of image I_i , or it might contain additional sources of error due to other causes. And define,

$$Q_i(x, y) \equiv \frac{1}{[\sigma_i(x, y)]^2}. \quad (6)$$

Then the error in $B(x, y)$ is given by,

$$\sigma[B(x, y)] = \sqrt{\sum_{i=1}^n \frac{[a_i(x, y)]^2}{Q_i}}. \quad (7)$$

Since the form of B is fixed, maximizing the S/N in B is equivalent to minimizing equation (7) subject to the constraints (eqs. [3]). It is straight forward to show (see Appendix) that this is accomplished when

$$a_i(x, y) = \frac{\langle A^2 Q(x, y) \rangle Q_i(x, y) - \langle A Q(x, y) \rangle A_i Q_i(x, y)}{n[\langle A^2 Q(x, y) \rangle \langle Q(x, y) \rangle - \langle A Q(x, y) \rangle^2]}, \quad (8)$$

where

$$\langle G(x, y) \rangle \equiv \frac{1}{n} \sum_{i=1}^n G_i(x, y). \quad (9)$$

It is not immediately obvious, but equations (8) reduces to equation (4) for the special case of $n = 2$. By direct substitution of equation (8) into equation (7),

$$\sigma[B(x, y)] = \frac{1}{\sqrt{n}} \left[\langle Q(x, y) \rangle - \frac{\langle A Q(x, y) \rangle^2}{\langle A^2 Q(x, y) \rangle} \right]^{-1/2}. \quad (10)$$

For the special case of $n = 2$, this becomes

$$\sigma[B(x, y)] = \frac{[A_2^2/Q_1(x, y) + A_1^2/Q_2(x, y)]^{1/2}}{|A_2 - A_1|}, \quad (11)$$

which confirms that for the case $n = 2$ it is best to choose images with the widest difference in magnifications. Indeed, even for the case $n > 2$, equation (8) shows that images at the extreme ranges of magnification are automatically given more weight than those with intermediate magnifications. To illustrate this concretely, we show in Figure 1 two cases, $Q \propto A^{-1}$ and constant Q , which are respectively appropriate for the limits where the magnified source is always above and always below the sky. We choose $n = 100$ and assume that the magnifications A_i are uniformly distributed between 1 and 20.

Of course, one could choose the coefficients a_i to be independent of position. In this case, one would apply equation (8) by adopting a set of Q_i that are representative of the images, for example the Q_i averaged over the PSF of the magnified source, or of the central pixel. However, there does not appear to be any compelling reason to do this. Moreover, the strong difference in the functional forms shown in Figure 1 implies that the optimal linear combinations may be very different near the center of the lensed source (which tends toward being above the sky) than they are near the wings (which tends toward being below the sky).

We note that an image of the (unmagnified) source, S , can also be constructed in a similar manner. Such an image may be useful when studying the image of the unlensed light. With alternative constraints

$$\sum_{i=1}^n a'_i(x, y) = 0; \quad \sum_{i=1}^n a'_i(x, y)A_i = 1, \quad (12)$$

one obtains in place of equations (5), (8), (10) and (11);

$$S = \frac{I_2 - I_1}{A_2 - A_1} \quad \text{for } n = 2, \quad (13a)$$

$$a'_i(x, y) = \frac{\langle Q(x, y) \rangle A_i Q_i(x, y) - \langle A Q(x, y) \rangle Q_i(x, y)}{n[\langle A^2 Q(x, y) \rangle \langle Q(x, y) \rangle - \langle A Q(x, y) \rangle^2]}, \quad (13b)$$

$$\sigma[S(x, y)] = \frac{1}{\sqrt{n}} \left[\langle A^2 Q(x, y) \rangle - \frac{\langle A Q(x, y) \rangle^2}{\langle Q(x, y) \rangle} \right]^{-1/2}, \quad (14a)$$

$$\sigma[S(x, y)] = \frac{[1/Q_1(x, y) + 1/Q_2(x, y)]^{1/2}}{|A_2 - A_1|} \quad \text{for } n = 2. \quad (14b)$$

3. Discussion

The method outlined in § 2 is likely to prove useful primarily in cases where the uncertainty in the photometric determination of blending is large, either because of intrinsic degeneracies or because the baseline is very faint. The first condition applies mainly to caustic-crossing binary lenses, while the second applies to high-magnification events. Caustic-crossing binaries are themselves a major source of high-magnification events, so binaries are the singled out for both reasons. The spectacular binary event MACHO 98-SMC-1, which had an extremely faint ($I \sim 22$) source and maximum magnification of $A \sim 100$, is an excellent example: five microlensing groups combined their precise and extensive data sets, but were still not able to distinguish between two solutions with values of F_b that differed by a factor of two (Afonso et al. 2000 and references therein).

However, the precise determination of the blending with the aid of image subtraction can also significantly impact generic high-magnification events, which play a major role in planet searches (Albrow et al. 2001; Gaudi et al. 2001). Such events are exceptionally sensitive to planetary companions of the primary lens, because both the planetary caustic (Gould & Loeb 1992) and the central caustic (Griest & Safizadeh 1998) are much more likely to cause planetary perturbations than in typical events. For this reason, these events are often monitored more intensively than typical events, which further increases the sensitivity of these events to planet detection. No planets have yet been discovered, but accurate estimates of the blending are essential to place upper limits on the presence of planets in the cases of non-detections. For example, Gaudi et al. (2001) excluded from their analysis all events where the uncertainty in the lens-source impact parameter was greater than 50% because these uncertainties

led to a significant (and difficult to determine) underestimation in the events’ sensitivity to planets. A 50% uncertainty in impact parameter corresponds to the difference between a model with $F_b = 0$ and one with $F_b = F_s$. (About one quarter of all the events included in their analysis had impact-parameter uncertainties greater than 25%.) Hence, even though the degeneracy is continuous in this case (as opposed to the discrete degeneracy discussed above for binaries), the uncertainty in the blending parameter F_b derived solely from the analysis of the light curve, can still be quite large. This implies that additional information about the blend acquired from the analysis of the images can be important in reducing or resolving the degeneracy.

How can such information be extracted? Primarily by investigating whether the unlensed light (or a significant component of it) has both the same color and the same position as the source. Recall that the source color can be determined very precisely by regression of the flux in two bands, while the source position can be determined very precisely using image subtraction.

More specifically, if the lens model has incorrectly estimated the flux of the lensed source, then it will attribute the difference between the true and estimated F_s to the blend parameter F_b . Thus, for instance, there may be no actual unlensed light, but an incorrect fit will yield a finite F_b . If F_b is significantly negative, the error of the model will be manifest. But if F_b is positive, then no such argument can be made. However, in this case one can still perform another test: an unlensed source that was inferred on the basis of an incorrect model would have exactly the same color as the lensed source. Hence, identical colors would be a strong hint of a wrong model. Unfortunately, this test is not definitive. On the one hand, an unlensed star could have the same color as the lensed source, so that a common color would not prove that the inferred unlensed light was an artifact. On the other hand, even if the color is found to be different, this would prove only that there was *some* real source of unlensed light but it would not prove that the model F_b was correct. That is, a significant (either positive or negative) fraction of the flux attributed by the model to unlensed light could still belong to the lensed source.

If the derived F_b is purely an artifact of the model, then the procedure outlined in § 2 will yield an isolated “unlensed source” with exactly the same position as the lensed source. The combination of this and the fact that it had the same color as the lensed source would be convincing proof that it was an artifact. On the other hand, a real unlensed source that was displaced from the lensed source by as little as $\sim 10\%$ of the PSF would easily be distinguishable from an artifact. For example, if this unlensed source was subtracted from a scaled image of the lensed source (see eqs. [13]), the result would be a “shadowed mountain” effect which is familiar from subtraction of misaligned images.

If the image of the unlensed light consisted of an isolated point source at the same position as the lensed source but having a different color from it, then one could conclude that this was probably the lens itself (or possibly a companion to the lens or source), since the chance of a random field star being aligned with the source to within $\lesssim 10\%$ of the seeing disk is small.

Of course, it is possible that there is more than one unlensed source, and if these are too closely packed together, it will be difficult to make sense of them, even with the lensed source removed. However, regardless of the configuration of the unlensed sources, it will be easier to disentangle them in the image with the lensed source removed, than it is in an image containing the lensed source. This will be especially true when all the sources are very faint. In this case, the high S/N image of the unlensed sources formed by combining many individual images will mark an exceptional improvement.

It is important to keep in mind that all the images that are combined to form an image of the unlensed light must be convolved to the *worst* seeing of the lot. Hence, there is an inevitable tradeoff in forming a high S/N image between increasing the S/N and decreasing the resolution. One should therefore rank order the images by seeing, and set the threshold at various values to determine which ensemble of images produces the best image of the unlensed light.

ACKNOWLEDGEMENTS

This work was supported in part by NSF grant AST 97-27520 and in part by JPL contract 1226901.

APPENDIX

A. Minimization with Constraints

We use Lagrange multipliers to evaluate the n -dimensional vector $\{\tilde{a}_i\}$ that minimizes the quadratic function $\mathcal{H}(\{a_i\}) = \sum_{i,j=1}^n b_{ij}(a_i - a_i^0)(a_j - a_j^0) + \mathcal{H}_0$, subject to the m constraints $\sum_{i=1}^n a_i \alpha_i^k = z^k$ ($k = 1, \dots, m$). Here the a_i^0 , the b_{ij} , and \mathcal{H}_0 are constants. At this minimum, $\nabla \mathcal{H}$ must lie in the m -dimensional subspace spanned by the constraint vectors $\{\alpha_i^k\}$, i.e., $\sum_{j=1}^n b_{ij}(\tilde{a}_j - a_j^0) + \sum_{l=1}^m D^l \alpha_i^l = 0$, or

$$\tilde{a}_i = a_i^0 - \sum_{l=1}^m D^l \kappa_i^l; \quad \kappa_i^l \equiv \sum_{j=1}^n c_{ij} \alpha_j^l, \quad (\text{A1})$$

where $(c_{ij}) \equiv (b_{ij})^{-1}$, and the D^l are constants to be determined. Multiplying equation (A1) by each of the α_i^k yields a set of m equations,

$$\sum_{l=1}^m C^{kl} D^l = \sum_{i=1}^n a_i^0 \alpha_i^k - z^k; \quad C^{kl} \equiv \sum_{i=1}^n \alpha_i^k \kappa_i^l = \sum_{i,j=1}^n c_{ij} \alpha_i^k \alpha_j^l, \quad (\text{A2})$$

which can be inverted to solve for the D^k ,

$$D^k = \sum_{l=1}^m B^{kl} \left(\sum_{i=1}^n a_i^0 \alpha_i^l - z^l \right); \quad (B^{kl}) = (C^{kl})^{-1}. \quad (\text{A3})$$

To obtain equation (8) in § 2, one sets $\mathcal{H}_0 = 0$, $a_i^0 = 0$, $b_{ij} = \delta_{ij}/Q_i$, $m = 2$, $\alpha_i^1 = 1$, $\alpha_i^2 = A_i$, $z^1 = 1$, $z^2 = 0$, and then substitutes into equations (A1) and (A3).

Note that for the special case where \mathcal{H} can be interpreted as χ^2 (not of direct concern here, but of general interest), c_{ij} is the covariance matrix of the unconstrained parameters a_i , i.e., $c_{ij} = \text{cov}(a_i, a_j) = \langle a_i a_j \rangle - \langle a_i \rangle \langle a_j \rangle$. One then finds by direct substitution that $\text{cov}(D^k, a_i^0) = \sum_{l=1}^m B^{kl} \kappa_i^l$, so that the covariances of the constrained parameters, $\tilde{c}_{ij} = \text{cov}(\tilde{a}_i, \tilde{a}_j)$, are given by

$$\tilde{c}_{ij} = c_{ij} - \sum_{k,l=1}^m B^{kl} \kappa_i^k \kappa_j^l. \quad (\text{A4})$$

To further specialize to an important subcase, let $\alpha_i^k = \delta_{ik}$. Then $\kappa_i^k = c_{ik}$ and $C^{kl} = c_{kl}$, hence $B^{kl} = \hat{b}_{kl}$, where $(\hat{b}_{kl}) = (\hat{c}_{kl})^{-1}$ and \hat{c}_{kl} is the (unconstrained) $m \times m$ covariance matrix restricted to the m parameters that are to be constrained. Thus, for this special case, equations (A1), (A3), and (A4) become

$$\tilde{a}_i = a_i^0 - \sum_{k,l=1}^m c_{ik} \hat{b}_{kl} (a_l^0 - z^l); \quad \tilde{c}_{ij} = c_{ij} - \sum_{k,l=1}^m \hat{b}_{kl} c_{ik} c_{jl}. \quad (\text{A5})$$

REFERENCES

- Afonso, C., et al. 2000, ApJ, 532, 340
- Alard, C. 2000, A&AS, 144, 363
- Alard, C., & Lupton, R. H. 1998, ApJ, 503, 325
- Alard, C., Mao, S., & Guibert, J. 1995, A&A, 300, L17
- Albrow, M. D., et al. 1999, ApJ, 522, 1022
- Albrow, M. D., et al. 2001, ApJ, 556, L113
- Alcock, C., et al. 2001, ApJ, 552, 582
- Boden, A. F., Shao, M., & van Buren, D. 1998, ApJ, 502, 538
- Dominik, M. 1999, A&A, 349, 108
- Dominik, M., & Sahu, S. 2000, ApJ, 534, 213
- Gaudi, B. S., et al. 2001, ApJ, 566, 000 (astro-ph/0104100)
- Gould, A., & Loeb, A. 1992, ApJ, 396, 104
- Griest, K., & Safizadeh, N. 1998, ApJ, 500, 37
- Jeong, Y., Han, C., & Park, S.-H. 1999, ApJ, 511, 569
- Han, C. 2001, MNRAS, submitted (astro-ph/0107543)
- Han, C., & Jeong, Y. 1999, MNRAS, 309, 404
- Tomaney, A. B., & Crotts, A. P. S. 1996, AJ, 112, 2872
- Woźniak P. R. 2000, Acta Astron., 50, 421

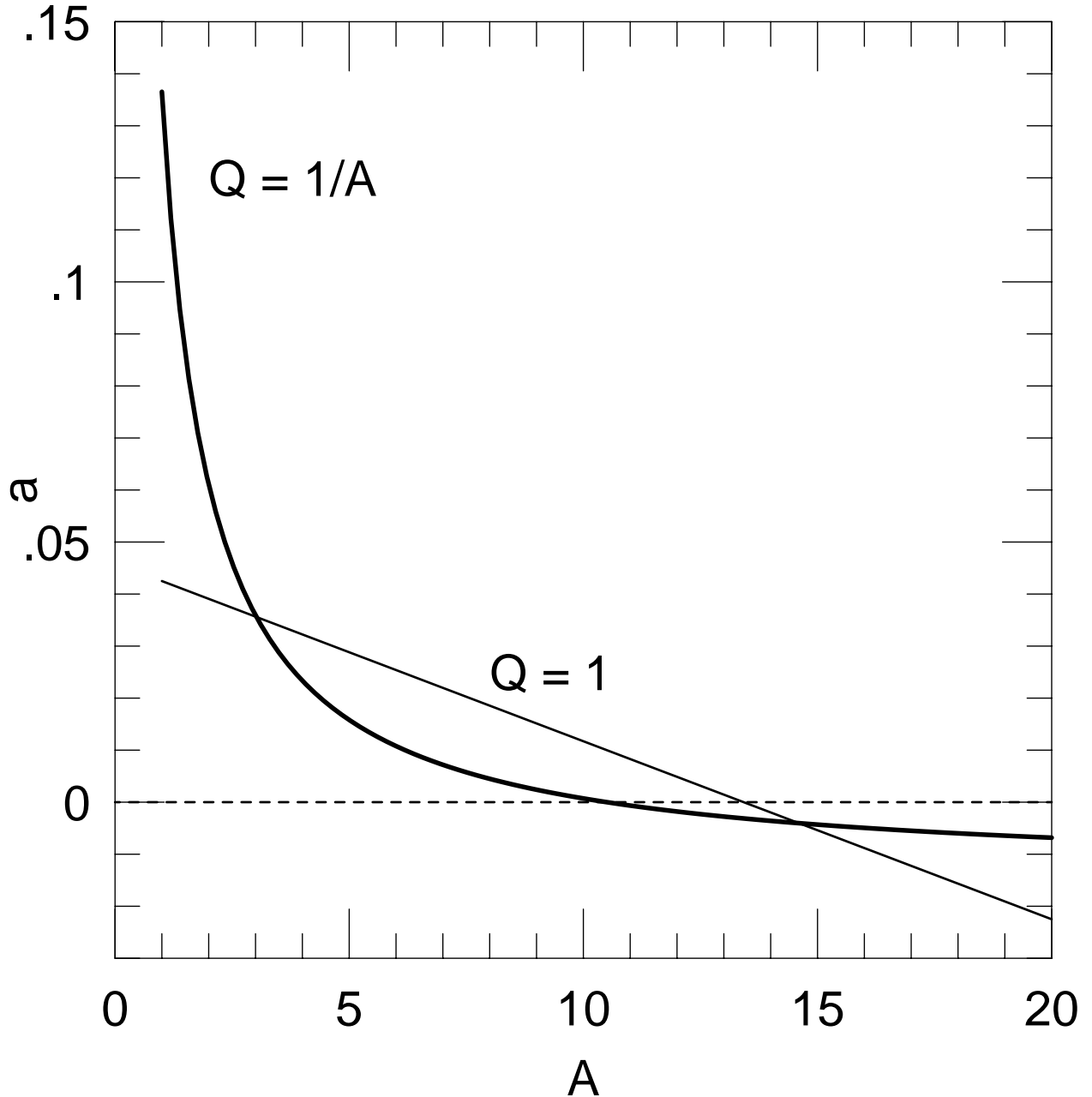


Fig. 1.— Optimal weighting factors, a , for combining images to produce a source-free image of the unlensed light in a microlensing event, as functions of the magnification, A , of each image. The examples shown are for a total of $n = 100$ images with magnifications uniformly distributed over the interval $1 \leq A \leq 20$. The solid line shows the factors for the case where the flux errors are independent of the magnification (constant Q), which is appropriate when even the highly magnified source is below the sky. The bold curve shows the factors for the case where the flux errors are proportional to the square root of the magnification ($Q \propto 1/A$), which is appropriate when the source itself is above the sky.